Ambient synthesis of a multifunctional 1D/2D hierarchical Ag-Ag2S nanowire/nanosheet heterostructure with diverse applications

Jinyan Xiong
University of Wollongong, jx513@uowmail.edu.au

Chao Han
University of Wollongong, ch861@uowmail.edu.au

Weijie Li
University of Wollongong, wl347@uowmail.edu.au

Qiao Sun
Soochow University, qsun@uow.edu.au

Jun Chen
University of Wollongong, junc@uow.edu.au

See next page for additional authors

Recommended Citation

Ambient synthesis of a multifunctional 1D/2D hierarchical Ag-Ag2S nanowire/nanosheet heterostructure with diverse applications

Abstract

A new type of unique 1D/2D hierarchical Ag-Ag2S heterostructures is fabricated by an extremely simple solution route under ambient conditions. The morphology, size, crystal structure and composition of the products were comprehensively investigated, and it was found that the reaction time and the amount of S powder play crucial roles in the formation of well-defined 1D/2D hierarchical Ag-Ag2S heterostructures. The diffusion and Ostwald ripening processes dominate the evolution of the heterostructure. The resultant 1D/2D Ag-Ag2S hybrids exhibit great potential in Li/Na ion battery anodes, SERS detection and decoloration towards organic dyes.

Keywords

Disciplines

Publication Details

Authors

Jinyan Xiong, Chao Han, Weijie Li, Qiao Sun, Jun Chen, Shulei Chou, Zhen Li, and S X. Dou

CrossMark
click for updates

Ambient synthesis of a multifunctional 1D/2D hierarchical Ag–Ag$_2$S nanowire/nanosheet heterostructure with diverse applications†

Jinyan Xiong,[a] Chao Han,[a] Weijie Li,[a] Qiao Sun,[b] Jun Chen,[c] Shulei Chou,[a] Zhen Li*[ab] and Shixue Dou[a]

A new type of unique 1D/2D hierarchical Ag–Ag$_2$S heterostructures is fabricated by an extremely simple solution route under ambient conditions. The morphology, size, crystal structure and composition of the products were comprehensively investigated, and it was found that the reaction time and the amount of S powder play crucial roles in the formation of well-defined 1D/2D hierarchical Ag–Ag$_2$S heterostructures. The diffusion and Ostwald ripening processes dominate the evolution of the heterostructure. The resultant 1D/2D Ag–Ag$_2$S hybrids exhibit great potential in Li/Na ion battery anodes, SERS detection and decoloration towards organic dyes.

Introduction

Semiconductor-noble metal-based hybrid nanostructures have promising potential in energy, environmental and catalysis applications, due to their unique optical, electrical and catalytic properties arising from each of their components and their synergistic interactions.[1] Their great potential drives engineering of nanofabrication and properties of such semiconductor–metal hybrid nanomaterials with different architectures.[2] Being one of the important semiconductor-noble metal hybrids, Ag–Ag$_2$S with different heterostructures, including nanotubes,[1a] nanowires,[3] nanoprisms,[4] and nanoparticles,[5] have been widely exploited in the past several years. It was reported that Ag–Ag$_2$S nanohybrids showed excellent properties in resistive switches,[3,6] DNA hybridization probes,[4b] bactericidal effects,[4a,5a,7] photodegradation of pollutants,[1a,5b] and water splitting.[6a] From the fabrication

perspective, most fabrications of Ag–Ag$_2$S hybrids suffered from the drawbacks of high temperature,[5b] complicated processes,[6a,7] and high energy consumption,[3] which seriously restrict their development and practical applications. It still remains a challenging but exciting topic to explore a facile strategy to prepare well-defined and unique multidimensional Ag–Ag$_2$S heterostructures, as well as to investigate their novel properties and potential applications.

Generally, the composition and structure of hybrids play the pivotal role in determining their functions and applications.[8] Recent advances demonstrate that complex one-dimensional/two-dimensional (1D/2D) heterostructures composed of 1D nanowires and 2D nanosheets exhibit great potential in photocatalysis,[9] energy storage,[10] counter electrodes,[11] and photoelectrochemical cells,[12] owing to their unique structural features, which allow them to transport charge carriers very well along the axial direction and have a relatively large surface area. However, to the best of our knowledge, there are sparse reports on the preparation of 1D/2D Ag–Ag$_2$S heterostructures and exploration of their fascinating properties. Herein, a new type of 1D/2D Ag–Ag$_2$S architecture has been fabricated by an extremely simple solution route under ambient conditions, and the as-synthesized Ag–Ag$_2$S hybrids exhibit favorable multifunctional properties for energy and environmental applications.

Experimental

Experimental methods

Ag nanowires (Ag NWs) were prepared according to our previous report with a minor modification.[13] In a typical synthesis, 10 mL of 1,2-propanediol containing PVP40 was loaded into a

^{a} *Institute for Superconducting & Electronic Materials, The University of Wollongong, NSW 2500, Australia. E-mail: zhenl@uow.edu.au*
^{b} *School of Radiation Medicine and Radiation Protection, Collaborative Innovation Center of Radiation Medicine of Jiangsu Higher Education Institutions, Soochow University, 199 Ren Ai Road, Suzhou Industrial Park, Suzhou 215123, China. E-mail: zhenli@suda.edu.cn*
^{c} *Intelligent Polymer Research Institute, The University of Wollongong, NSW 2500, Australia*

† Electronic supplementary information (ESI) available: EDX spectrum and SEM image of the as-synthesized 1D/2D Ag–Ag$_2$S heterostructures; TEM image and HRTEM image of the product prepared with a S to Ag ratio of 0.2 : 1; XRD patterns of the products prepared with different molar ratios of sulfur powder to Ag nanowires; SEM images and XRD pattern of the Ag–Ag$_2$S heterostructures obtained after 6 days; XRD pattern and SEM images of the Ag–Ag$_2$S nanoparticles and pure Ag$_2$S nanoparticles; SERS spectra of MB solutions with different concentrations adsorbed on the 1D/2D hierarchical Ag–Ag$_2$S hybrid heterostructures. See DOI: 10.1039/c5ce02134k

25 mL vial, and heated with magnetic stirring in an oil bath at 135 °C for 1 h. 1 mL of NaCl in 1,2-propanediol solution (1 mM) was then quickly added, and stirred for another 5 min. Finally, $AgNO_3$ (0.1 M solution in 1,2-propanediol) was added to the mixture. The mixture solution was then heated at 135 °C with magnetic stirring for 1 h, yielding the gray Ag NWs.

Ag nanoparticles (Ag NPs) were prepared by the similar procedure applied to Ag NWs, except without NaCl.

1D/2D Ag–Ag$_2$S hierarchical heterostructures were prepared from the above synthesized Ag nanowires and sulphur powder. 8 mL of freshly prepared Ag NW solution was firstly added into 10 mL of ethanol under constant magnetic stirring for 10 min. Then, 0.0048 g of sulfur powder was added into the reaction mixture. The reaction mixture was stirred for 24 h, and then the resultant Ag–Ag$_2$S precipitate was separated by centrifugation, washed with de-ionized water and absolute ethanol several times to remove impurities, and then dried at 60 °C.

Ag–Ag$_2$S heteronanoparticles were prepared using the similar approach to the 1D/2D Ag–Ag$_2$S hierarchical heterostructures, except 8 mL of Ag NPs solution was added rather than Ag NWs solution.

Pure Ag$_2$S nanospheres were prepared from $AgNO_3$ and saturated Na_2S solution in ethanol in the presence of PVP. The reaction mixture was stirred for 24 h.

Characterization

X-Ray diffraction (XRD) measurements were performed on a GBC MMA X-ray diffractometer using Cu Kα_1 radiation (40 kV). XRD patterns were recorded from 20° to 80° with a scanning rate of 4° min^{-1}. SEM images were collected using a field-emission scanning electron microscope (JSM-7500FA, JEOL) operated at an accelerating voltage of 5 kV. TEM images were collected on a field-emission transmission electron microscope (ARM-200 F, JEOL), using an accelerating voltage of 200 kV. Ultraviolet/visible (UV/vis) absorption spectra were recorded at room temperature on a UV-3600 (Shimadzu) spectrometer.

SERS measurement

2 mg of the as-synthesized 1D/2D Ag–Ag$_2$S hierarchical heterostructures were added into 200 μL of MB solution with concentrations of 10^{-3}, 10^{-4}, 10^{-5}, and 10^{-6} M. The mixture was ultrasonically dispersed for 10 min and shaken for 12 h in the dark at room temperature. Then, the dispersion was dropped onto a glass slide for SERS measurement. All SERS spectra were collected on a JY HR 800 Raman spectrometer under excitation at 632 nm with a power of 13.5 mW.

Battery performance measurements

The electrode slurry for lithium/sodium ion batteries was prepared by mixing 70 wt% active powder material, 15 wt% carbon black, and 15 wt% carboxymethyl cellulose (CMC) binder. The slurry was pasted on copper foil, followed by drying in a vacuum oven overnight at 80 °C, and then pressing

at a pressure of 30 MPa to enhance the contact between the mixture and the copper foil. For the lithium ion battery test, lithium foil was employed as both the reference and counter electrodes. The electrolyte was 1 M LiPF$_6$ in ethylene carbonate (EC)–diethyl carbonate (DEC) solution (1:1 v/v). For the sodium ion battery test, sodium foil was cut by the doctor blade technique from bulk sodium stored in mineral oil, which then was employed as both the reference and counter electrodes. The electrolyte was 1 M NaClO$_4$ in EC/DEC solution (1:1 v/v). The cells were assembled in an argon-filled glove box, and their electrochemical performance was tested with the Land test system in the voltage range of 0–2.5 V with a current density of 30 mA g^{-1}.

Decoloration test

The application of the as-synthesized 1D/2D Ag–Ag$_2$S hierarchical heterostructures for the decoloration of organic dyes was evaluated in both a dark environment and under solar light irradiation. In the experiment, 50 mg of the heterostructures were added into 50 mL of MB solution (10^{-5} M) at room temperature. After ultrasonic dispersion, the suspension was stirred in the dark for 30 min to ensure the establishment of an adsorption–desorption equilibrium between the hybrid structures and MB. Then, the solution was exposed to irradiation of a LSC-100 solar simulator (Newport) under magnetic stirring. At each irradiation time interval, 2 mL of the suspension was collected and then centrifuged to remove the photocatalysts. The concentration of MB was analyzed by using a Shimadzu UV-3600 spectrophotometer, and the characteristic absorption of MB at 664 nm was used to evaluate the decoloration activity. All of the measurements were carried out at room temperature.

Results and discussion

A typical Ag–Ag$_2$S architecture is synthesized through the reaction of Ag nanowires (NWs) with sulfur powder in ethanol at room temperature. The X-ray diffraction (XRD) pattern of the as-prepared sample in Fig. 1A indicates that the product is a hybrid consisting of monoclinic Ag$_2$S (JCPDS card no. 14–0072) and face-centered cubic Ag (JCPDS card no. 04–0783). The absence of impurity peaks in the XRD pattern suggests the high purity of the Ag–Ag$_2$S hybrid synthesized by this facile approach. The energy-dispersive X-ray (EDX) analysis result shown in Fig. S1 in the (ESI†) indicates that the as-prepared hybrid is composed of Ag and S with an atomic ratio (*i.e.* Ag/S) higher than the stoichiometric ratio of 2:1 for Ag$_2$S, demonstrating the successful synthesis of the Ag–Ag$_2$S hybrid.

Characterizations by scanning electron microscopy (SEM) and transmission electron microscopy (TEM) provide insight into the morphology and detailed structure of the as-prepared Ag–Ag$_2$S hybrid. A panoramic view of the as-prepared sample shows uniform nanowires ~100 nm in diameter and several micrometers in length (Fig. S2†). The enlarged SEM image in Fig. 1B reveals that many sheet-like
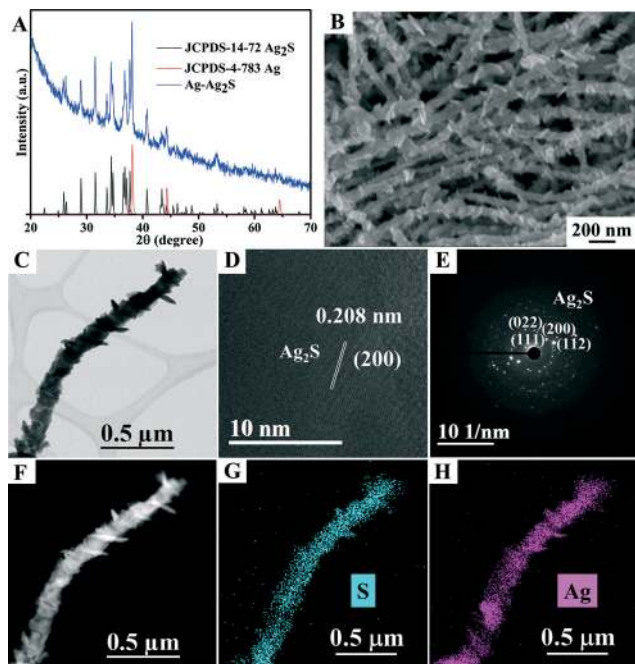
Fig. 1 (A) XRD pattern and (B) SEM image of the as-prepared Ag–Ag$_2$S heterostructures with a S/Ag ratio of 1 : 2; (C) TEM image, (D) HRTEM image, (E) SAED pattern, (F) HAADF image, and (G, H) the corresponding EDX elemental mapping analysis of an individual Ag–Ag$_2$S heterostructure.

nanostructures (~15 nm in thickness) have densely grown on the entire surface of the 1D nanowire to form a 1D/2D hierarchical nanostructure. Fig. 1C clearly shows the TEM image of an individual 1D/2D Ag–Ag$_2$S hierarchical nanostructure, in which sheet-like leaves surround the 1D nanowire in a three-dimensional (3D) manner. The hybrid has two kinds of segments with different contrasts, in which the darker segment is metallic Ag and the brighter segment should be semiconducting Ag$_2$S. The high-resolution TEM (HRTEM) image in Fig. 1D shows a lattice fringe of 0.208 nm, which corresponds to the (200) plane of monoclinic Ag$_2$S. The selected area electron diffraction (SAED) pattern (Fig. 1E) also reveals the presence of Ag$_2$S in the hybrid. High-angle annular dark-field (HAADF) imaging was used to identify each chemical component. Due to the differences between Ag and S in scattering electrons, the as-prepared Ag–Ag$_2$S hybrid has different contrasts in the HAADF image (Fig. 1F), which is opposite to those observed in the bright field image, *i.e.* the bright segments indicate the presence of the heavier metal Ag, and the dark parts indicate the presence of Ag$_2$S. Elemental mapping of a single 1D/2D heterostructure obtained by HAADF-TEM reveals the homogeneous distribution of Ag and S elements in the hybrid (Fig. 1G and H).

The above results demonstrate the successful synthesis of 1D/2D Ag–Ag$_2$S hierarchical heterostructures. To understand the formation mechanism of such an interesting structure, we carried out time-dependent experiments and collected samples at different time intervals. The morphological and structural evolution of the products obtained with different reaction times were examined by SEM (Fig. 2). Before the

addition of S powder, the Ag NWs are very straight, and the surfaces are very smooth (Fig. 2A). After the addition of S powder and reaction for 30 min, no significant difference was observed on the surfaces of the Ag NWs at this early stage (Fig. 2B), although the reaction mixture changed from grey to yellow due to the formation of a thin Ag$_2$S layer on the surfaces of the NWs. As the reaction proceeded for 1.5–4 h, the surfaces of the nanowires became rougher, and a few spiny or scaly structures were formed, as shown in Fig. 2(C–E). The epitaxial growth of the Ag$_2$S nanostructures could be due to the excessive crystallization of Ag$_2$S in some places on the surface of the nanowire. When the reaction time was lengthened to 6–8 h, more and more quasi-nanosheets were formed on the nanowires to form a mace-like structure, as shown in Fig. 2(F and G). With a further extended reaction time, the nanosheets adhering to the nanowires became larger and became joined to one another (Fig. 2H). After the reaction for 24 h, the final products were entirely composed of the 1D/2D hybrid heterostructures (Fig. 2I).

These structures and morphologies were further analyzed by TEM and high-resolution TEM. As shown in Fig. 3A, the TEM images confirm that for the products obtained within 30 min, a thin Ag$_2$S layer is coated on the surface of the Ag NWs to form a well-defined core–shell Ag–Ag$_2$S nanowire with a relatively smooth surface, due to the sulfuration of the Ag NWs. The corresponding HRTEM image (Fig. 3B) clearly reveals that the resolved lattice fringes are 0.199 nm, corresponding to the *d*-spacing of the (−131) planes of monoclinic Ag$_2$S. With the growth of the Ag$_2$S shell, the surface of the hetero-nanowires became coarse [Fig. 3(C and D)]. Further prolonging the reaction time to 6 h led to the formation of a mace-like structure with a few quasi-nanosheets on the nanowires [Fig. 3(E and F)].

The crystalline structures and optical properties of the above products were further studied and the results are shown in Fig. 4. The XRD patterns (Fig. 4A) clearly reveal that
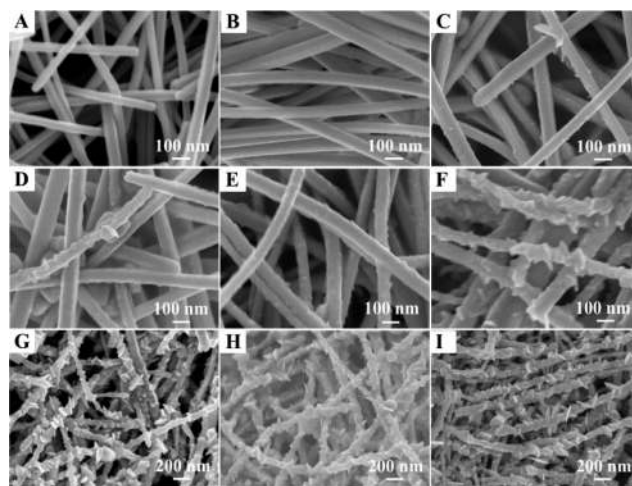
Fig. 2 SEM images of Ag–Ag$_2$S heterostructures obtained with a S/Ag ratio of 1 : 2 at different reaction times: (A) 0 min, (B) 30 min, (C) 1.5 h, (D) 2 h, (E) 4 h, (F) 6 h, (G) 8 h, (H) 12 h, and (I) 24 h.
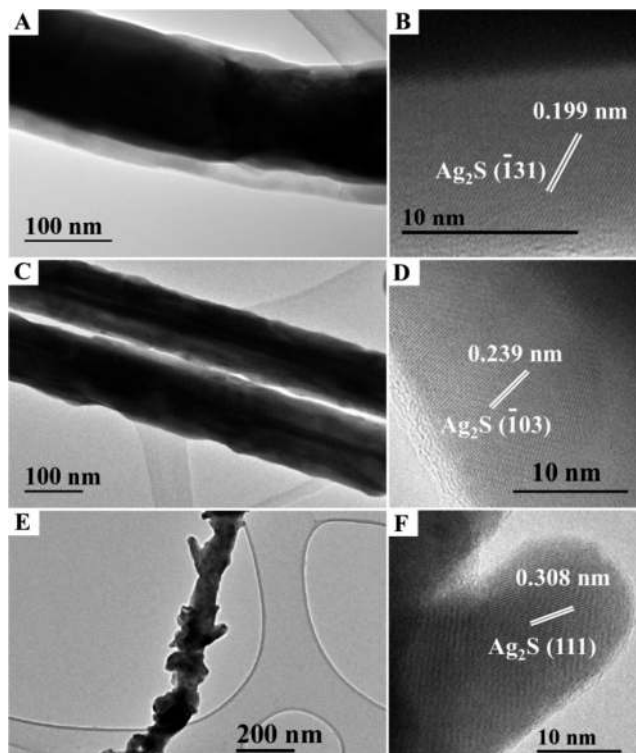
Fig. 3 TEM images (A, C, and E) and corresponding HRTEM images (B, D, and F) of Ag–Ag$_2$S heterostructures obtained at different reaction times: (A, B) 30 min, (C, D) 4 h, and (E, F) 6 h.

the intensity of the Ag$_2$S diffraction peaks are gradually increased with increasing reaction time, demonstrating the gradual formation of the Ag–Ag$_2$S hybrid and the increased content of Ag$_2$S. It is well known that Ag NWs show intense surface plasmon resonance (SPR) absorption in the visible region, which is highly sensitive to their diameter and length-to-diameter ratio, as well as the optical and electronic properties of their surroundings.[13,14] The absorption spectra shown in Fig. 4B were from ethanol-Ag and ethanol-Ag/Ag$_2$S dispersions collected at different reaction times, which were measured with a UV-3600 (Shimadzu) spectrometer in the UV-vis-NIR region at room temperature. The scan speed is medium and the interval is 1 nm. The pure Ag NWs exhibit two absorbance peaks at 350 and 385 nm. The peak at 350 nm could be attributed to the longitudinal mode of the nanowires,
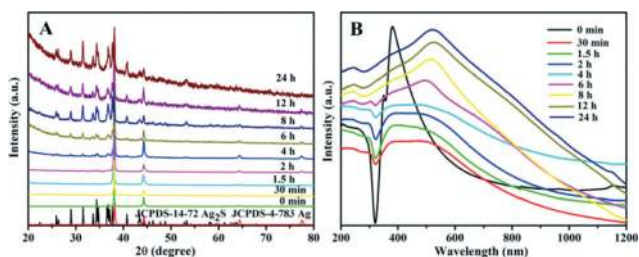

Fig. 4 (A) XRD patterns and (B) UV-vis-NIR absorption spectra of Ag–Ag$_2$S heterostructures obtained with a S/Ag ratio of 1 : 2 at different reaction times.

which is similar to that of bulk Ag[14a,15] or the out-of-plane quadrupole resonance of Ag NWs.[16] The peak at 385 nm is assigned to the transverse plasmon resonance of Ag NWs.[14a,15] The optical response of the Ag NWs was observed to be markedly affected by the formation of Ag$_2$S. Upon the formation of the Ag$_2$S shell (30 min), the longitudinal mode almost disappeared and the transverse plasmon resonance of the Ag cores observed at about 385 nm decreased, redshifted and significantly broadened, which could have possibly contributed to the synergistic effects between Ag NWs and the Ag$_2$S shell in the Ag–Ag$_2$S hybrids: the higher refractive index of Ag$_2$S (1.9–2.5)[17] than that of ethanol (~1.359)[14a,18] and its high relative dielectric constant ($\varepsilon_r = 6$),[19] as well as the confinement of free electrons within the Ag core.[14a,20] The peak width of the SPR band increased slightly with increasing time (30 min–4 h), which implies that the Ag nanowires are becoming more isolated with less and less electronic interactions between nearby unites. When the reaction time is 6 h, the spectra exhibited a new absorption band centered at around 495 nm and a very weak SPR peak. The new absorption is ascribed to the band gap of Ag$_2$S, which is similar to the reported absorption between 490–520 nm of rod-like Ag$_2$S nanocrystals,[21] 530 nm of Ag$_2$S nanofibers,[6c] 573 nm of Ag$_2$S nanotubes,[22] 443 nm of Ag$_2$S nanoparticle chains,[23] and 514–531 nm of the Ag$_2$S/Ag heterostructures.[7] The weak SPR observed herein indeed suggested that the good contact between the Ag$_2$S and Ag segments might ensure an effective charge transfer across the phase boundary, and changes in the structure and shape of the product. When the time was increased to 8 h, the SPR absorption bands of the Ag NWs almost disappeared owing to their further sulfuration, and the characteristic absorption feature of Ag$_2$S moved to the longer wavelength region at around 515 nm. The observed red-shifts may reflect the grain/crystallite growth of Ag$_2$S and enlargement of the Ag$_2$S domains in the heterostructures. Eventually, with more and more quasi-nanosheets formed on the nanowires (see Fig. 2G and H), the characteristic absorption feature of Ag$_2$S moved to around 525 nm for the time at 12 h, providing strong evidence that essentially Ag NWs have turned into Ag–Ag$_2$S hybrids and the product mainly composed of Ag$_2$S components. The final dispersion was brownish black in appearance. The Ag–Ag$_2$S NWs obtained at 24 h exhibit a similar absorption profile in comparison with the products obtained at 12 h, in which the characteristic absorption feature of Ag$_2$S remained at 525 nm and did not shift with increasing reaction time, due to the lack of obvious changes in the structures and shapes of the final products (see Fig. 2I). Their broad absorbance from the UV to the near-infrared window is crucial for the full use of sunlight.

It should be noted that the formation of the 1D/2D Ag–Ag$_2$S hierarchical heterostructures is strongly dependent on the Ag/S ratio. Fig. 5 presents the SEM images of the Ag–Ag$_2$S heterostructures obtained from different ratios of Ag/S after the reaction for 24 h. The surfaces of the heterostructures become smoother and smoother with the decreasing S/Ag ratio from 0.4 : 1 (Fig. 5A) to 0.33 : 1 (Fig. 5B), to 0.22 : 1 (Fig. 5C)
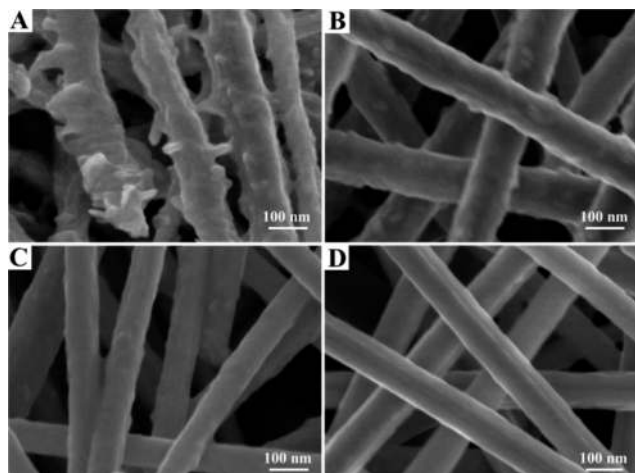
Fig. 5 SEM images of Ag–Ag$_2$S heterostructures prepared with different molar ratios of sulfur powder to Ag nanowires: (A) 0.4:1, (B) 0.33:1, (C) 0.22:1, and (D) 0.2:1.

and to 0.2:1 (Fig. 5D). For the heterostructures obtained from the ratio of 0.2:1, the morphology of the initial Ag NWs remains almost unchanged, except for the formation of a thin Ag$_2$S layer on the surface of the Ag NWs, as shown by the TEM and HRTEM images in Fig. S3†(A and B).

Based on these results, the formation of the 1D/2D Ag–Ag$_2$S hierarchical heterostructures can be illustrated in Scheme 1A, in which the diffusion and Ostwald ripening processes dominate the evolution of the heterostructure morphology. It is well known that room temperature diffusion of metals into semiconductors to form metal–semiconductor
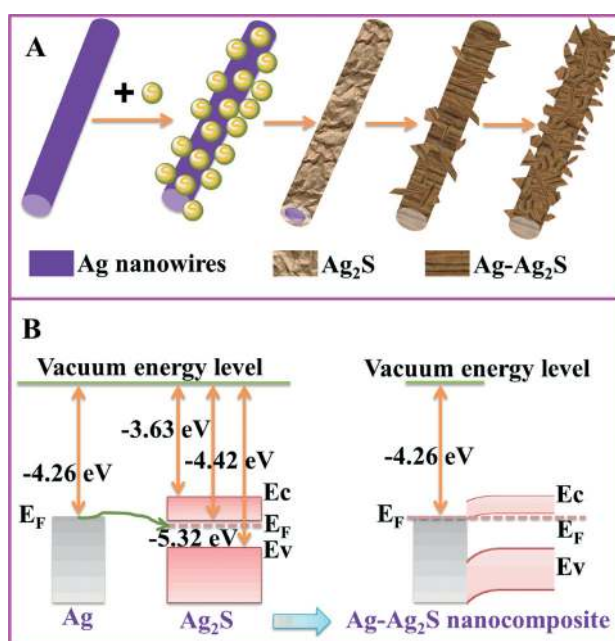
Scheme 1 (A) Schematic illustration of the synthesis of 1D/2D Ag–Ag$_2$S heterostructures and (B) simplified band structures in the Ag–Ag$_2$S system before and after contact.

pairs generally occurs on the nanometer scale when the band-gap energy of the semiconductor is lower than about 2.5 eV.[2b,24] The band gap of a bulk Ag$_2$S crystal is about 0.9 eV at room temperature, and 1.4–2.3 eV for its nanoscale analogues.[2b,7] Therefore, the diffusion of Ag metal in the Ag–Ag$_2$S nanowires well satisfies the aforementioned diffusion criterion. Scheme 1B shows a simplified diagram of the energy level of the Ag–Ag$_2$S nanocomposites and the work function of Ag, the dominant energy level, the bottom of the conduction band and the top of the valence band of Ag$_2$S, which are −4.26 eV, −3.63 eV, −4.42 eV and −5.32 eV, respectively, from the vacuum energy level.[2b,7,25] In equilibrium, the Fermi levels of Ag and Ag$_2$S should be at the same level. According to the potential alignment, the electrons (majority carriers) can drift from the Fermi level of Ag to the Fermi level (E_F, which is approximately treated as the donor level) of the n-type Ag$_2$S semiconductor upon their contact, leaving some positive charge buildup on the metal contact interface,[7,26] which could facilitate the diffusion of Ag in Ag$_2$S and result in substitutional interstitial processes.[25] As a consequence, the Ag–Ag$_2$S interface causes the bending and upshift of the energy bands.[26] In the presence of S powder, which could serve as a strong oxidant, the surface reactive Ag atoms of the nanowires are oxidized to form a thin uniform Ag$_2$S layer at an early stage. The subsequent diffusion of Ag would continue, as well as its reaction with S at different sites, leading to the growth of convexity due to the increase in internal energy arising from the interfacial strain caused by the lattice mismatch between Ag and Ag$_2$S, and due to the large volume expansion during the sulfurization reaction, since the molar volumes of Ag and Ag$_2$S are 10.3 cm^3 mol^{-1} and 34.3 cm^3 mol^{-1}, respectively.[19a] The initially formed Ag$_2$S convexity continues its growth and undergoes an Ostwald ripening process to turn into nanosheets. With the growth of Ag$_2$S, the diffusion of Ag atoms from the internal Ag core to the surface Ag$_2$S becomes slower and slower, leading to a negligible difference in the 1D/2D hybrid heterostructures obtained after 24 h. The SEM images and XRD pattern of a sample reacted for 6 days are shown in Fig. S4,† which are similar to those obtained at 24 h. Compared to previously reported methods for the fabrication of 1D Ag–Ag$_2$S heterostructures, a major advantage of the present work is the use of the stable sulfur powder rather than Na$_2$S to synthesize this new type of well-defined 1D/2D hybrid architecture under ambient conditions.[4b,27]

As a proof-of-concept application of this intriguing hybrid nanostructure, the obtained 1D/2D hierarchical Ag–Ag$_2$S heterostructures were used as multifunctional materials in rechargeable Li/Na-ion batteries, in decolouration of organic dyes, as well as in surface-enhanced Raman spectroscopy (SERS) detection. Fig. 6A shows the cycling performance and coulombic efficiency of the electrodes in Li-ion batteries fabricated from the 1D/2D hierarchical Ag–Ag$_2$S heterostructures. Their capacities drop in the first few cycles due to the formation of a solid electrolyte interphase (SEI) film, which is similar to what happens in other nanostructure-based electrodes.[28] The first few cycles involve the formation
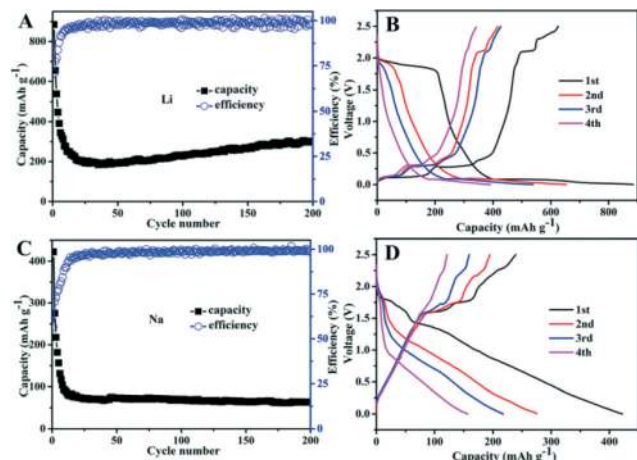
Fig. 6 Cycling performance and charge–discharge voltage profiles for the first 4 cycles of the 1D/2D hierarchical Ag–Ag$_2$S heterostructure electrode used as the anode for the lithium ion battery (A and B) and the sodium ion battery (C and D) at a specific current of 30 mA g^{-1}.

of a stable SEI film resulting from electrolyte decomposition, which degrades the capacity. The capacity slowly decreases to around 201 mAh g^{-1} after 25 cycles of charging and discharging, followed by a gradual increase to 302 mAh g^{-1} after 200 cycles. The increasing trend in the capacity is similar to that in the reported literature, and the capacity is larger than that of pure Ag$_2$S nanoparticles.[29]

From the charge–discharge curves in Fig. 6B, the initial discharge and charge capacities are 885 and 626 mA h g^{-1}, respectively, corresponding to a coulombic efficiency of 71%, which is higher than that of the reported Ag$_2$S/C nanocomposite (~61%) and pure Ag$_2$S (~40%), and the charge capacity of the Ag–Ag$_2$S heterostructure electrode was also larger than that of the other two.[29] Nevertheless, the coulombic efficiency increased to above 98% after 25 cycles, suggesting the excellent retention capacity of the Ag–Ag$_2$S electrode with 1D/2D morphology. These electrochemical characteristics can be attributed to their composition and unique 1D/2D structure: (1) the Ag in the hybrid possesses much better electrical conductivity than the pure Ag$_2$S and provides interconnected charge pathways so that the conductivity and mechanical strength of the whole heterostructure electrode are improved; (2) the 1D nanowires with superior electronic conductivity and the 2D nanosheets effectively shorten the diffusion length of the Li ions in the small primary subunits;[30] (3) the unique hierarchical 1D/2D structure could not only provide more sites or paths for lithium ion storage or transport, but also provides enough space to buffer the volume expansion during cycling and facilitate good contact with the conductive carbon black.[31]

In addition to the lithium ion battery, the 1D/2D hierarchical Ag–Ag$_2$S heterostructure electrode was also used as the anode for the sodium ion battery for the first time. As shown in Fig. 6C and D, its capacity decreased dramatically from 422 to 91 mAh g^{-1} in the first 10 cycles, followed by a gradual decrease to 63 mAh g^{-1} after 200 cycles. The initial discharge

and charge capacities are 422 and 239 mA h g^{-1}, respectively, corresponding to a coulombic efficiency of 57%, and the coulombic efficiency increased to above 98% after 30 cycles, which also suggests the excellent capacity retention of the Ag–Ag$_2$S electrode with 1D/2D morphology.

Fig. 7A shows the removal of methylene blue (MB) by the 1D/2D Ag–Ag$_2$S hierarchical heterostructures under both visible light illumination and in dark conditions. Approximately 76% of the dye is decolorized under solar light exposure of 150 min as compared to the 69% efficiency in dark conditions, demonstrating the weak photocatalytic effect of the 1D/2D Ag–Ag$_2$S hierarchical heterostructures (Fig. 7B). It is also implied, however, that the adsorption process is quicker than the photodegradation process. Ag$_2$S works more as an adsorbent and less as a photosensitizer and electron donor in imparting the decoloration effects to the Ag NWs under solar light irradiation. The adsorption process transfers MB molecules to the photocatalyst surfaces, but the solar-light-driven photocatalysis process cannot radically eliminate MB. Compared with the Ag–Ag$_2$S nanoparticles (Fig. 7C and Fig. S5 in the ESI†), pure Ag$_2$S nanoparticles (Fig. 7D and S6 in the ESI†), and Ag NWs, the excellent decoloration of MB on the 1D/2D Ag–Ag$_2$S hierarchical heterostructures can be ascribed to their strong adsorption capability in the dark, due to the interfacial effect after the introduction of Ag$_2$S nanosheets onto the surface of the Ag NWs, and the weak photodegradation of the adsorbed MB molecules through the heterostructures.

Surface-enhanced Raman scattering (SERS) spectroscopy is a powerful tool for the detection of traces of chemical and biological species. To study the SERS responses of our as-prepared 1D/2D hierarchical Ag–Ag$_2$S heterostructures, the commonly used organic dye methylene blue (MB) was selected as the target molecule. The original Raman spectrum of MB is dominated by ν(C–C) ring stretching at ~1622 cm^{-1},
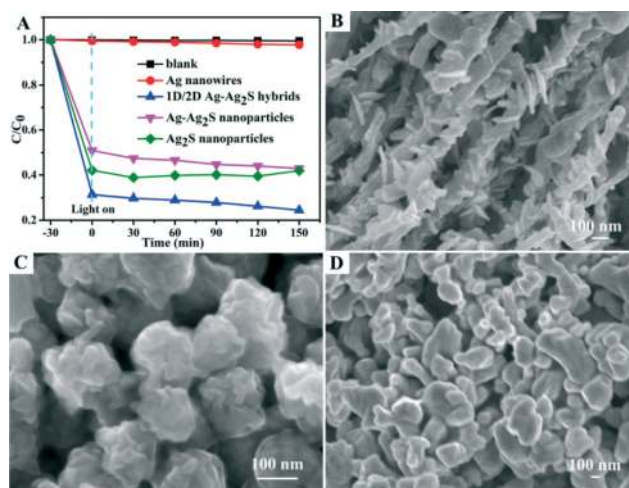

Fig. 7 (A) Decoloration activity of the 1D/2D hierarchical Ag–Ag$_2$S compared with the Ag–Ag$_2$S nanoparticles and pure Ag$_2$S nanoparticles and SEM images of 1D/2D hierarchical Ag–Ag$_2$S (B), Ag–Ag$_2$S nanoparticles (C) and pure Ag$_2$S nanoparticles (D).
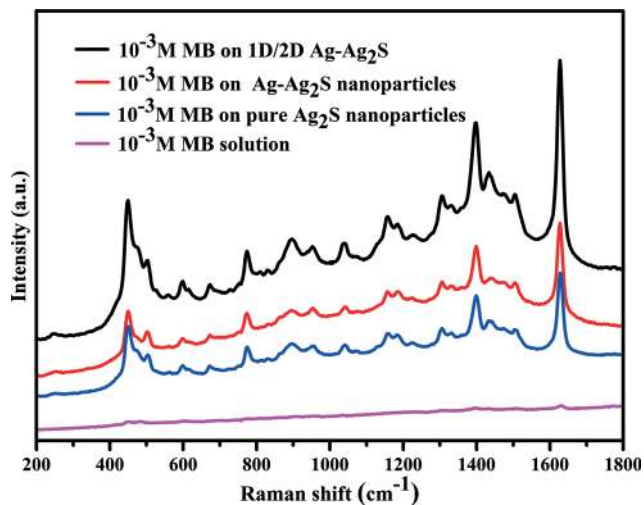
Fig. 8 SERS spectra of the 1D/2D hierarchical Ag–Ag$_2$S compared with Ag–Ag$_2$S nanoparticles and pure Ag$_2$S nanoparticles.

α(C–H) in-plane ring deformation at $\sim$1398 cm^{-1}, and δ(C–N–C) skeletal deformation at $\sim$449 cm^{-1}.[32] Fig. 8 shows the Raman spectra of MB deposited on different glass slides coated with 1D/2D hierarchical Ag–Ag$_2$S nanowires, Ag–Ag$_2$S nanoparticles, and pure Ag$_2$S nanoparticles, in comparison with the spectrum of MB. It is obvious that most signals of the characteristic peaks were highly enhanced in the SERS spectra compared with that of the MB solution (10^{-3} M). The characteristic peaks of MB are located almost in the same place or only slightly shifted, which indicates the adsorption of MB on the substrate surface. According to the peak at $\sim$1626 cm^{-1}, the signal enhanced by the 1D/2D hierarchical Ag–Ag$_2$S heterostructures and the Ag–Ag$_2$S nanoparticles is higher than that by the pure Ag$_2$S nanoparticles, which demonstrates the significant role of Ag in the hybrid structure in enhancement. It is generally accepted that both electromagnetic enhancement and chemical enhancement could contribute to the overall surface enhancement.[33] The unique strong local plasmon resonance from the Ag metal in the hybrid structure generates more "hot spots" that can contribute to SERS enhancement, compared to the pure Ag$_2$S nanoparticles.[34] The highest intensity in the case of the 1D/2D hierarchical Ag–Ag$_2$S heterostructures is probably due to the hierarchical and concave structures constructed from 1D nanowires and 2D nanosheets, which may boost their enhancement in comparison with spherical nanoparticles with smooth surfaces.[33,35] The enhancement of pure Ag$_2$S nanoparticles is relatively weaker, since the localized surface plasmon resonance (LSPR) of Ag$_2$S is usually located in the near-infrared/infrared region, and SERS enhancement mainly results from the charge transfer resonance between the Ag$_2$S and MB molecules.[4b,33,34,36]

In order to demonstrate the application of the as-fabricated 1D/2D hierarchical Ag–Ag$_2$S as a promising SERS-active substrate, we also examined the dependence of the SERS signal on the concentration of adsorbed MB (Fig. S7†). The intensity of the spectra increases with the increase in concentration from 10^{-6} M to 10^{-3} M. At low concentrations (*i.e.* 10^{-5}/10^{-6} M), the characteristic peaks of MB at $\sim$1622 cm^{-1}, $\sim$1398 cm^{-1} and $\sim$449 cm^{-1} are faintly visible, and they become much more prominent and sharp at higher concentrations (*i.e.* 10^{-4}–10^{-3} M). This result is probably due to more dye molecules adsorbed on the substrate surface, which can create more surface active "hot spots" compared to lower concentrations.

Conclusions

In summary, unique 1D/2D hierarchical Ag–Ag$_2$S heterostructures were successfully prepared at room temperature by an extremely simple solution method. The growth of Ag–Ag$_2$S hybrids is dominated by the diffusion and Ostwald ripening processes. The resultant 1D/2D hierarchical Ag–Ag$_2$S heterostructures exhibit good capacity when used as Li/Na ion battery anodes, high sensitivity for the detection of organic dyes through SERS, and decoloration activity towards organic dyes. It was expected that this work could open up new avenues towards the facile and rational synthesis of multifunctional 1D/2D hierarchical architectures of semiconductor-noble metal hybrids for diverse applications.

Acknowledgements

Notes and references

1 (*a*) W. Yang, L. Zhang, Y. Hu, Y. Zhong, H. B. Wu and X. W. Lou, *Angew. Chem., Int. Ed.*, 2012, **51**, 11501; (*b*) S. T. Kochuveedu, Y. H. Jang and D. H. Kim, *Chem. Soc. Rev.*, 2013, **42**, 8467; (*c*) X. Huang, Z. Zeng, S. Bao, M. Wang, X. Qi, Z. Fan and H. Zhang, *Nat. Commun.*, 2013, **4**, 1444.

2 (*a*) W.-T. Chen, Y.-K. Lin, T.-T. Yang, Y.-C. Pu and Y.-J. Hsu, *Chem. Commun.*, 2013, **49**, 8486; (*b*) X. Hong, Z. Yin, Z. Fan, Y.-Y. Tay, J. Chen, Y. Du, C. Xue, H. Chen and H. Zhang, *Small*, 2014, **10**, 479; (*c*) Z. Fan, X. Zhang, J. Yang, X.-J. Wu, Z. Liu, W. Huang and H. Zhang, *J. Am. Chem. Soc.*, 2015, **137**, 10910.

3 G. R. Bourret and R. B. Lennox, *Nanoscale*, 2011, **3**, 1838.

4 (*a*) S. Xiong, B. Xi, K. Zhang, Y. Chen, J. Jiang, J. Hu and H. C. Zeng, *Sci. Rep.*, 2013, **3**, 2177; (*b*) B. Liu and Z. Ma, *Small*, 2011, **7**, 1587.

5   (*a*) X. Ma, Y. Zhao, X. Jiang, W. Liu, S. Liu and Z. Tang, *ChemPhysChem*, 2012, **13**, 2531; (*b*) F. Jiang, Q. Tian, M. Tang, Z. Chen, J. Yang and J. Hu, *CrystEngComm*, 2011, **13**, 7189.

6   (*a*) Y. Li, X. Ye, Y. Ma and L. Qi, *Small*, 2015, **11**, 1183; (*b*) C. Liang, K. Terabe, T. Hasegawa and M. Aono, *Nanotechnology*, 2007, **18**, 485202; (*c*) H. Wang and L. Qi, *Adv. Funct. Mater.*, 2008, **18**, 1249.

7   M. Pang, J. Hu and H. C. Zeng, *J. Am. Chem. Soc.*, 2010, **132**, 10771.

8   (*a*) J. Hu, A. Liu, H. Jin, D. Ma, D. Yin, P. Ling, S. Wang, Z. Lin and J. Wang, *J. Am. Chem. Soc.*, 2015, **137**, 11004; (*b*) C. Yuan, H. B. Wu, Y. Xie and X. W. Lou, *Angew. Chem., Int. Ed.*, 2014, **53**, 1488; (*c*) C. Lan, J. Gong and Y. Jiang, *J. Alloys Compd.*, 2013, **575**, 24; (*d*) C. Lan, J. Gong, Y. Jiang and Q. Ding, *CrystEngComm*, 2012, **14**, 8063.

9   W. Zhou, Z. Yin, Y. Du, X. Huang, Z. Zeng, Z. Fan, H. Liu, J. Wang and H. Zhang, *Small*, 2013, **9**, 140.

10 J. Liu, J. Jiang, C. Cheng, H. Li, J. Zhang, H. Gong and H. J. Fan, *Adv. Mater.*, 2011, **23**, 2076.

11 X. Q. Chen, Z. Li, Y. Bai, Q. Sun, L. Z. Wang and S. X. Dou, *Chem. – Eur. J.*, 2015, **21**, 1055.

12 B. Xu, P. He, H. Liu, P. Wang, G. Zhou and X. Wang, *Angew. Chem., Int. Ed.*, 2014, **53**, 2339.

13 J. Xiong, Z. Li, J. Chen, S. Zhang, L. Wang and S. Dou, *ACS Appl. Mater. Interfaces*, 2014, **6**, 15716.

14 (*a*) P. Ramasamy, D.-M. Seo, S.-H. Kim and J. Kim, *J. Mater. Chem.*, 2012, **22**, 11651; (*b*) R. Jin, Y. Cao, C. A. Mirkin, K. L. Kelly, G. C. Schatz and J. G. Zheng, *Science*, 2001, **294**, 1901.

15 (*a*) Z. Wang, J. Liu, X. Chen, J. Wan and Y. Qian, *Chem. – Eur. J.*, 2005, **11**, 160; (*b*) Y. Sun, B. Gates, B. Mayers and Y. Xia, *Nano Lett.*, 2002, **2**, 165.

16 (*a*) S. Chen and D. L. Carroll, *Nano Lett.*, 2002, **2**, 1003; (*b*) R. Jin, Y. Charles Cao, E. Hao, G. S. Metraux, G. C. Schatz and C. A. Mirkin, *Nature*, 2003, **425**, 487; (*c*) Y. Gao, L. Song, P. Jiang, L. F. Liu, X. Q. Yan, Z. P. Zhou, D. F. Liu, J. X. Wang, H. J. Yuan, Z. X. Zhang, X. W. Zhao, X. Y. Dou, W. Y. Zhou, G. Wang, S. S. Xie, H. Y. Chen and J. Q. Li, *J. Cryst. Growth*, 2005, **276**, 606.

17 (*a*) D. Okoli, G. Okeke and A. Ekpunobi, *Pac. J. Sci. Tech.*, 2010, **11**, 411; (*b*) Y.-T. Long and C. Jing, *Localized Surface Plasmon Resonance Based Nanobiosensors*, Springer, Berlin Heidelberg, 2014; (*c*) J. Zhu, Y. Shen, A. Xie and L. Zhu, *J. Mater. Chem.*, 2009, **19**, 8871.

18 T. Hirakawa and P. V. Kamat, *J. Am. Chem. Soc.*, 2005, **127**, 3928.

19 (*a*) J. Zeng, J. Tao, D. Su, Y. Zhu, D. Qin and Y. Xia, *Nano Lett.*, 2011, **11**, 3010; (*b*) S. Chang, Q. Li, X. Xiao, K. Y. Wong and T. Chen, *Energy Environ. Sci.*, 2012, **5**, 9444.

20 R. T. Tom, A. S. Nair, N. Singh, M. Aslam, C. L. Nagendra, R. Philip, K. Vijayamohanan and T. Pradeep, *Langmuir*, 2003, **19**, 3439.

21 Y. Zhao, D. Zhang, W. Shi and F. Wang, *Mater. Lett.*, 2007, **61**, 3232.

22 X. Fu, H. Zou and L. Zhou, *J. Nanosci. Nanotechnol.*, 2010, **10**, 5851.

23 D. Li, H.-Z. Xie, J.-K. Liu and C.-J. Duan, *J. Exp. Nanosci.*, 2011, **6**, 209.

24 (*a*) T. Mokari, A. Aharoni, I. Popov and U. Banin, *Angew. Chem., Int. Ed.*, 2006, **45**, 8001; (*b*) L. Xu, Z. Yin, S.-W. Cao, Z. Fan, X. Zhang, H. Zhang and C. Xue, *Chem. – Eur. J.*, 2014, **20**, 2742.

25 (*a*) J. Yang and J. Y. Ying, *Angew. Chem., Int. Ed.*, 2011, **50**, 4637; (*b*) J. Yang and J. Y. Ying, *J. Am. Chem. Soc.*, 2010, **132**, 2114.

26 Y. Li, L. Li, Y. Gong, S. Bai, H. Ju, C. Wang, Q. Xu, J. Zhu, J. Jiang and Y. Xiong, *Nano Res.*, 2015, **8**, 3621.

27 D. Seo, C. I. Yoo, J. Jung and H. Song, *J. Am. Chem. Soc.*, 2008, **130**, 2940.

28 (*a*) C. Han, Z. Li, W.-j. Li, S.-l. Chou and S.-x. Dou, *J. Mater. Chem. A*, 2014, **2**, 11683; (*b*) S. Zhang, W. Li, B. Tan, S. Chou, Z. Li and S. Dou, *J. Mater. Chem. A*, 2015, **3**, 4793.

29 Y. Hwa, C.-M. Park and H.-J. Sohn, *J. Electroanal. Chem.*, 2012, **667**, 24.

30 X. Xu, B. Dong, S. Ding, C. Xiao and D. Yu, *J. Mater. Chem. A*, 2014, **2**, 13069.

31 S. Chen, Y. Xin, Y. Zhou, F. Zhang, Y. Ma, H. Zhou and L. Qi, *J. Mater. Chem. A*, 2014, **2**, 15582.

32 (*a*) W. Liu, P. Miao, L. Xiong, Y. Du, X. Han and P. Xu, *Phys. Chem. Chem. Phys.*, 2014, **16**, 22867; (*b*) W. Jin, P. Xu, L. Xiong, Q. Jing, B. Zhang, K. Sun and X. Han, *RSC Adv.*, 2014, **4**, 53543.

33 Q. Kuang and S. Yang, *CrystEngComm*, 2014, **16**, 4940.

34 Q. Cao, R. Che and N. Chen, *Chem. Commun.*, 2014, **50**, 4931.

35 C. Qiu, L. Zhang, H. Wang and C. Jiang, *J. Phys. Chem. Lett.*, 2012, **3**, 651.

36 (*a*) J. R. Lombardi and R. L. Birke, *J. Phys. Chem. C*, 2008, **112**, 5605; (*b*) L. Jiang, P. Yin, T. You, H. Wang, X. Lang, L. Guo and S. Yang, *ChemPhysChem*, 2012, **13**, 3932.